Fuel retention in WEST and ITER divertors based on FESTIM monoblock simulations

Rémi Delaporte-Mathurin, Hao Yang, Julien Denis, James Dark, Etienne Hodille, Gregory de Temmerman, Xavier Bonnin, Jonathan Mougenot, Yann Charles, Hugo Bufferand, et al.

Fuel retention in WEST and ITER divertors based on FESTIM monoblock simulations

Rémi Delaporte-Mathurin[a,b,*], Hao Yang[a], Julien Denis[c], James Dark[b], Etienne A. Hodille[a], Gregory De Temmerman[d,e,f], Xavier Bonnin[d], Jonathan Mougenot[b], Yann Charles[b], Hugo Bufferand[a], Guido Ciraolo[a], Christian Grisolia[a]

[a] *CEA, IRFM/GCFPM, F-13108 Saint-Paul-lez-Durance, France*
[b] *Université Sorbonne Paris Nord, Laboratoire des Sciences des Procédés et des Matériaux, LSPM, CNRS, UPR 3407, F-93430, Villetaneuse, France*
[c] *Aix-Marseille Univ., CNRS, PIIM, F-13013 Marseille*
[d] *ITER Organization, Route de Vinon sur Verdon, CS 90 046, 13067, St Paul Lez Durance Cedex, France*
[e] *Zenon Research, 16 rue Séguier, 75006 Paris, France*
[f] *MINES ParisTech, Université PSL, Institut des Hautes Etudes pour l'Innovation et l'Entrepreneuriat (IHEIE), 75006 Paris, France*

Abstract

The influence of the input power, puffing rate and neutral pressure on the fuel (hydrogen isotopes) inventory of the WEST and ITER divertors is investigated. For the chosen range of parameters (relatively low temperature at the strike points), the inventory of the WEST divertor evolves as the power 0.2 of the puffing rate and as the power 0.3 of the input power. The inventory at the strike points is highly dominated by ions whereas it is dominated by neutrals in the private zone. Increasing the fuelling rate increases the retention in the private zone and decreases slightly the retention at the strike points. Increasing the input power increases the inventory at the strike points and does not affect much the inventory at the private flux region. The inventory of the ITER divertor is not strongly dependent on the divertor neutral pressure. The inventory increases from 0 Pa to 7 Pa and then decreases slightly from 7 Pa to 10 Pa. After 10^7 s of continuous exposure, the maximum inventory in the ITER divertor was found to be 14 g. The inventory is not maximum at the strike points due to the high surface temperature of the monoblocks in this region. The maximum accumulation of H in the ITER divertor is below 5 mg per 400 s discharge and below 2 mg per 400 s discharge after 200 discharges.

Keywords: Hydrogen transport, divertor, SolEdge3X-EIRENE, SOLPS, FESTIM

1. Introduction

Hydrogen isotopes (H[1]) transport in tokamaks is a crucial issue for several reasons. First, for safety reasons, the total inventory of radioactive material trapped in the reactor must be limited to a certain amount. In ITER, the limit of tritium in the vacuum vessel is 1 kg [1]. Second, outgassing of hydrogen from the monoblocks composing the divertor and from the tokamak first wall can reduce the plasma performances [2]. Finally, the lifespan of plasma facing components can be reduced due to hydrogen-induced damage (including embrittlement [3]).

Numerical modelling of H transport and retention in and outgassing from plasma facing components [4, 5, 6, 7] is therefore often required in order to tackle both issues. These simulations are supported by experimental work to determine key properties of fusion materials. H transport in monoblocks has been studied in 1D [8]. However, it was shown in [9] that the 2D edge effects had to be considered to have a better estimate of the H retention in the actively cooled divertor monoblocks. A recent major effort has been made to perform multi-dimensional simulations [9, 4, 5, 10].

In a previous study [4], the finite element code FESTIM [9, 5] was employed to simulate H isotopes transport in ITER-like monoblocks with the geometry given in [11] coupled to heat transfer. A novel method was developed to rapidly estimate the H inventory in the whole ITER divertor from plasma code results without having to run additional finite element simulation. Instead, a behaviour law relying on a data base of 600 FESTIM simulations correlates the H inventory in a monoblock to its surface temperature and surface concentrations (using a gaussian regression process as described in [12]).

The current work applies this technique to estimate the H inventory in the divertors of WEST and ITER based on SolEdge3X-EIRENE [13] and SOLPS-ITER [14] plasma simulations, respectively. The influence of control param-

*Corresponding author
Email address: remi.delaporte-mathurin@cea.fr ()
[1] H will be used to refer to all isotopes and mainly tritium

eters such as the input power, the puffing rate and the divertor neutral pressure is investigated.

2. Methodology

The H inventory of the WEST and ITER divertors will be computed by making use of a database of FESTIM simulations of H transport in ITER-like monoblocks from which a behaviour law is extracted using a gaussian regression process from the inference-tools python package [12]. These simulations model H transport in monoblocks for a fixed plasma exposure duration of 10^7 s. This corresponds to approximately 25 000 concatenated ITER discharges of 400 s each. As shown in [15], this approximation does not affect the H inventory in monoblocks with the current conditions.

These results (details can be found in [4]) are then interfaced with the exposure conditions obtained with the plasma simulations performed with the codes SOLPS [14] and SOLEDGE [13].

2.1. Plasma simulations

In this Section, the set-ups for the computation of the plasma exposure parameters are described. For the SolEdge3X-EIRENE runs, the puff rate and the input power were used as control parameters. For SOLPS-ITER calculation, the divertor neutral pressure is the control parameter.

2.1.1. SolEdge3X-EIRENE runs

The experimental WEST discharge #54903 in L-mode with a relatively stable plasma in the time window 7.9-8.1 s is selected for 2D simulations performed by SOLEDGE3X-EIRENE transport code (v588.165). A pure Deuterium plasma without drift effects is assumed. In order to make the simulations results comparable with experimental results, the simulation set-up is based on the real-time plasma state in the selected time window. For instance, the Lower-Single-Null magnetic configuration used for the simulation corresponds to the time-averaged configuration over the considered period (see Figure 1). The Scrape Off Layer input power is estimated by substracting the core radiated power (0.22 MW) inside the core-edge interface from the total heating power (0.764 MW). The radiated power in the core plasma is calculated by the bolometer method [16]. As no impurity is assumed in the simulation, the computed radiated power is expected to be lower when compared to reality. In order to get as many divertor conditions as possible, the puff rate was varied from 4.5×10^{20} molecule s^{-1} to 4.72×10^{21} molecule s^{-1} and the input power from 0.449 MW to 2.5 MW. The other setup parameters of the simulation are listed in Table 1. R_{wall} is the recycling coefficient of main chamber wall, R_{pump} is the recycling coefficient of the pump, D_{m} is the cross-field mass diffusivity perpendicular to the flux surface, ν is the momentum diffusivity, χ_e and χ_i are the heat flux diffusivity for electrons and ions, respectively. The gas puff position is set inside the private region and the pump position is set under the baffle (see Figure 1). The values of R_{wall} and R_{pump} are chosen to match the gas puff levels in the experiment. Classic transport coefficients in L-mode WEST plasmas are applied to match experimental target profiles. The simulation result shows a good agreement with the data from the experiment.

Table 1: Setup parameters used in the SOLEDGE3X simulations

Plasma composition	Deuterium, no impurity
Recycling coefficients	$R_{\text{wall}} = 0.99$ $R_{\text{pump}} = 0.95$
SOL input power	from 0.449 MW to 2.5 MW
Gas puff rate	from 4.5×10^{20} molecule s^{-1} to 4.72×10^{21} molecule s^{-1}
Drifts	-
Transport coefficients	$D_{\text{m}} = 0.3\ m^2\ s^{-1}$ $\nu = 0.3\ m^2\ s^{-1}$ $\chi_e = \chi_i = 1.0\ m^2\ s^{-1}$

2.1.2. SOLPS runs

Several ITER cases were taken with divertor neutral pressures varying from 1.8 Pa to 11.2 Pa. These SOLPS [14] scenarios can be found in the ITER Integrated Modelling Analysis Suite (IMAS) database [17, 18]. The nine simulations used in this work are labelled 122396, 122397, 122398, 122399, 122400, 122401, 122402, 122403 and 122404. These have been run in baseline burning plasma conditions (Q=10) and with an averaged separatrix Ne concentration of around 0.6 % [19].

2.2. Application to divertors

The distribution of the exposure conditions (angles of incidence, particles energies, particles fluxes and heat flux) are produced by SOLEDGE/SOLPS along the divertors of WEST and ITER (see Figures 1 and 3). These exposure conditions are converted into distributions of surface temperature T_{surface} and surface hydrogen concentration c_{surface} by Equations (1) and (2).

$$T_{\text{surface}} = 1.1 \times 10^{-4} \varphi_{\text{heat}} + T_{\text{coolant}} \quad (1)$$

where φ_{heat} is the surface heat flux in W m^{-2} and $T_{\text{coolant}} = 323$ K is the coolant temperature.

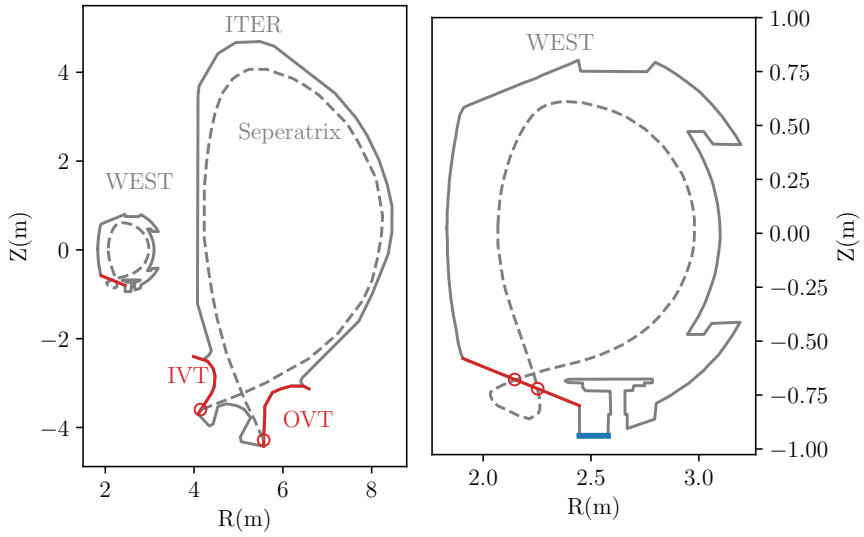

Figure 1: Geometry of WEST and ITER divertors showing the divertors in red, the plasma seperatrix and the location of the strike points. IVT and OVT stand for Inner and Outer Vertical Target, respectively. For WEST, the pump position (in blue) is under the baffle.

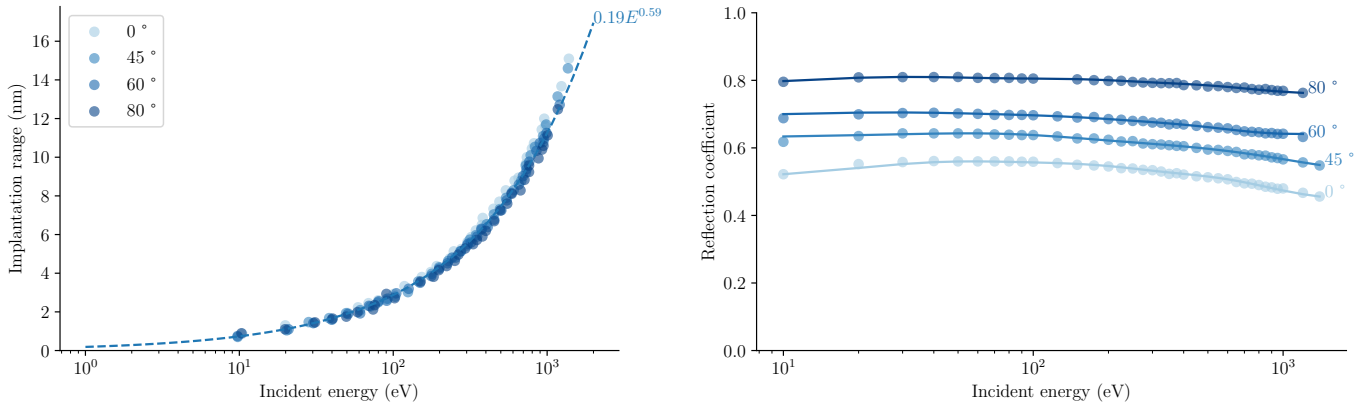

(a) Implantation range R_p

(b) Reflection coefficient r

Figure 2: Evolution of the implantation range and the reflection coefficient as a function of incident energy E and angle of incidence computed from SRIM simulations.

The relation between the heat flux φ_{heat} and the surface temperature T_{surface} (see Equation (1)) has been obtained from heat transfer simulations of ITER monoblocks [4].

The relation between the surface concentration of mobile H c_{surface} (m^{-3}), the particle flux $\varphi_{i\in\{\text{ions,atoms}\}}$ and T_{surface} is given by:

$$c_{\text{surface}} = (1 - r_{\text{atoms}}) \frac{R_{p,\text{atoms}}\ \varphi_{\text{atoms}}}{D(T_{\text{surface}})} + (1 - r_{\text{ions}}) \frac{R_{p,\text{ions}}\ \varphi_{\text{ions}}}{D(T_{\text{surface}})} \quad (2)$$

where the reflection coefficients r_i and implantation depths $R_{p,i}$ in m depend on the particle energy and angle of incidence (see Figure 2) and computed with SRIM [20], φ_i are the particles fluxes in $\text{m}^{-2}\,\text{s}^{-1}$ and $D(T)$ is the H diffusion coefficient in $\text{m}^2\,\text{s}^{-1}$. The implantation range and reflection coefficient were calculated with deuterium ions (mass of 2.014 and hydrogen species) on a W target. The deviation between protium, deuterium and tritium was below the angstrom for the range of energy used in this work.

According to the behaviour law obtained in [4], the temporal evolution of the H inventory along the divertors can be estimated from the surface concentration of mobile H and surface temperature (see Figure 3).

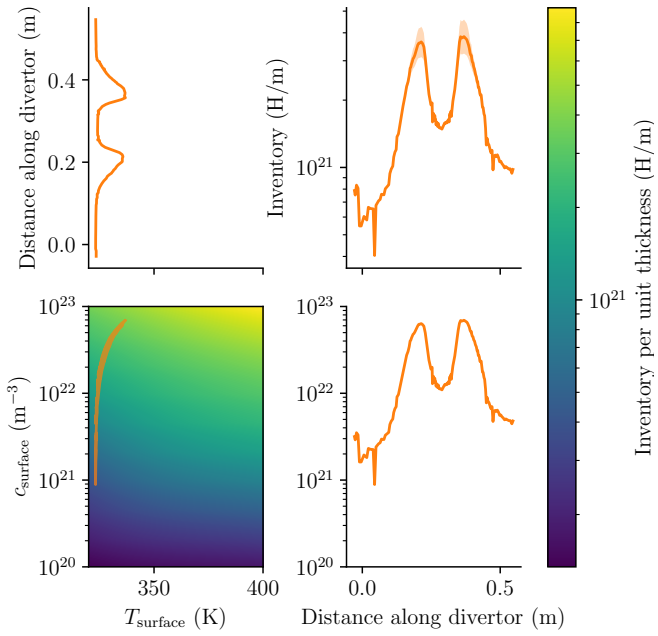

Figure 3: Method of H inventory estimation based on the surface concentration, the surface temperature and the behaviour law obtained in [4]. First T_{surface} (top left) and c_{surface} (bottom right) are calculated with equations 1 and 2 from the plasma simulation outputs. Then, both are reported on the behaviour law (bottom left) to estimate the inventory for the various position in the divertor (top right). The area corresponds to the 95% confidence interval computed by the Gaussian regression.

The relation between the implantation range R_p and the incident energy and angle of incidence can be obtained from SRIM [20] results (see Figure 2a). It was found that the angle of incidence had low influence on the implantation range. R_p can then be expressed (in m) as a function of the incident energy only (see Equation (3)).

$$R_p = 1.9 \times 10^{-10} E^{0.59} \tag{3}$$

where E is the incident energy in eV.

The evolution of the reflection coefficient r can also be estimated with SRIM for a perfect surface. The reflection coefficient varies from around 0.5 at 0 ° to 0.8 at 80 ° (see Figure 2b). According to [18], the incident angles for ions and atoms were assumed to be 60 ° and 45 °, respectively. It should be noted that since SRIM is based on the binary collision approximation, values around 10 eV might not be fully valid.

The source-code of the tool described in this work (divHretention) is under version control and openly available via Github under a MIT licence [21]. The divHretention python package is distributed via PyPi [22].

3. Results

All the computations have been made for very long exposure times (10^7 s) in order to better visualise trends. Even though cycling can have an effect on H outgassing at the monoblock plasma facing surface, it was shown in [15] that the evolution of the monoblock inventory with the fluence was not affected. Moreover, it can be shown that the divertors inventories evolve with a power law dependence of time.

3.1. WEST

Two parametric studies were performed on the WEST divertor varying the input power and the puffing rate. In this Section, the inner and outer strike points are located at 0.2 m and 0.36 m respectively (see Figure 1).

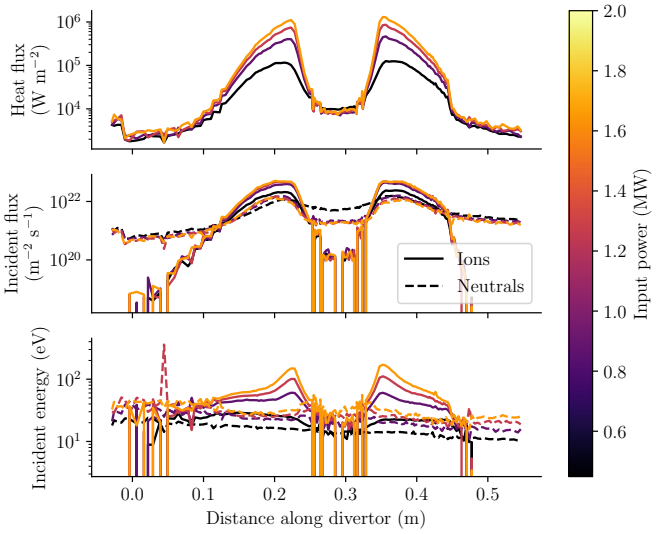

Figure 4: Distribution of heat flux, particle flux and particle energy along the WEST divertor computed by SOLEDGE3X-EIRENE with input powers varying from 0.49 MW to 2.0 MW with a puffing rate of 2.5×10^{21} molecule s^{-1}.

3.1.1. Power scan

The SOL input power was varied between 0.45 MW and 2.0 MW. Two puffing rate values were used: 2.5×10^{21} molecule s^{-1} and 4.4×10^{21} molecule s^{-1}.

The heat flux at the strike points increased with the input power from 0.1 MW m−2 to 10 MW m^{-2} (see Figure 4). The incident flux of particle was not significantly affected by the input power variation. The particle incident energy however increased up to 100 eV at the strike points.

The maximum retention was found to be located at the strike points (see Figure 5). The inventory at the outer strike point was higher than at the inner strike point. The retention at the strike points was found to increase with the SOL input power whereas it slightly decreased in the private zone (see Figure 6a). This was explained by an attachment of the plasma decreasing the particle flux in the private zone. Since the surface temperature is constant, this leads to a decrease in the surface concentration of hydrogen as seen on Figure 5. On the other hand, the increasing temperature at the strike points only enhanced

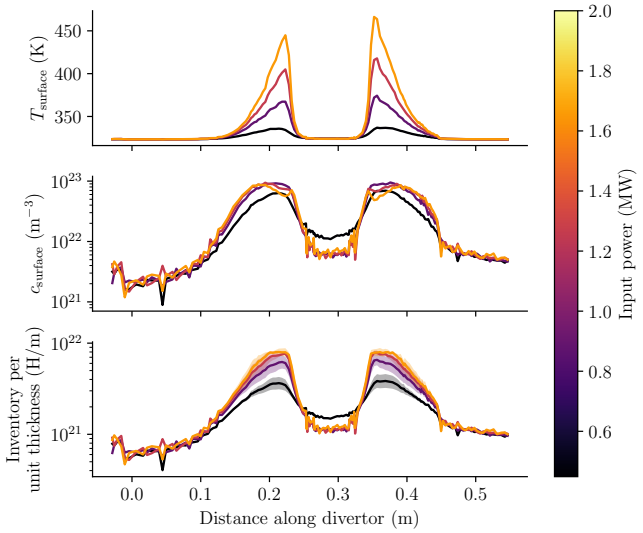

Figure 5: Distribution of surface temperature T_{surface}, surface concentration c_{surface} and inventory along the WEST divertor with input powers varying from 0.49 MW to 2.0 MW with a puffing rate of 2.5×10^{21} molecule s^{-1}.

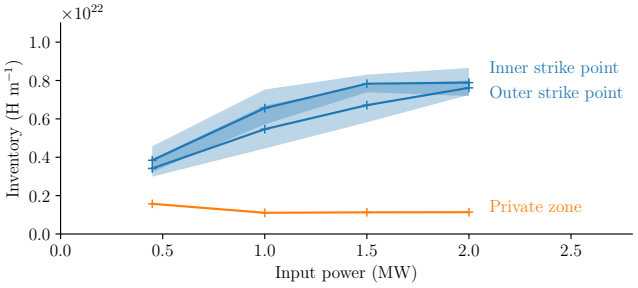

(a) Inventory per unit thickness after 10^7 s of exposure. The area corresponds to the 95% confidence interval.

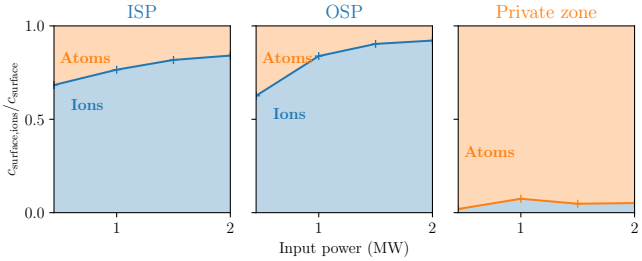

(b) Contribution of ions to the surface concentration of H. ISP and OSP stand for Inner Strike Point and Outer Strike Point respectively.

Figure 6: H inventory at the strike points and in the private zone as a function of the SOL input power with a puffing rate of 2.5×10^{21} molecule s^{-1}.

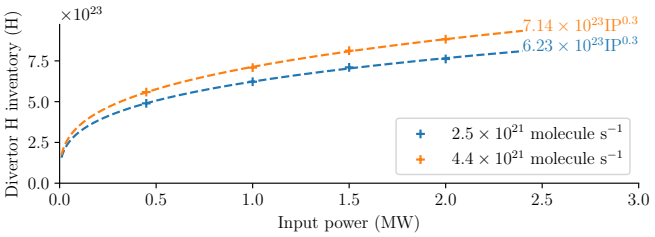

Figure 7: Evolution of the WEST divertor inventory as a function of SOL input power (IP) for several puffing rates.

the diffusion process while remaining low enough so that hydrogen could get trapped.

The total inventory in the WEST divertor is computed as follows:

$$\text{inv}_{\text{divertor}} = N_{\text{PFU}} \cdot \int \text{inv}_{\text{PFU}}(x)\, dx \tag{4}$$

where $N_{\text{PFU}} = 480$ is the number of PFU (Plasma Facing Units) in WEST, inv_{PFU} is the inventory per unit thickness in H m^{-1} (see Figure 5) and x the distance along the target in m.

At the strike points, the retention is dominated by the ion flux whereas neutrals are dominant in the private zone (see Figure 6b). The contribution of ions at the strike points increased with the input power but remained approximately constant in the private zone.

The divertor inventory increased with the input power (see Figure 7) and evolved as the power 0.3 of the input power. The maximum divertor inventory was 8.8×10^{23} H at 2.0 MW of SOL input power. This value of input power is still relatively low. Increasing the puffing rate lead to an increase in the inventory. This will be explained more thoroughly in Section 3.1.2.

The divertor inventory was found to increase as a square root of time.

3.1.2. Density scan

A parametric study on the puffing rate was performed. The puffing rate was varied between 4.4×10^{20} molecule s^{-1} and 4.7×10^{21} molecule s^{-1}. The SOL input power was fixed to 0.45 MW.

The heat flux was found to increase with the puffing rate in the private region, whereas it decreases at the strike points (see Figure 8). The particle flux on the other hand, increases with the puffing rate in every region, especially for the neutral particles. The incident energy of particles decreased with the puffing rate.

The maximum retention was again located at the strike points for all puffing rates values (see Figure 9). The inventory at the outer strike point was higher than at the inner strike point. The inventory in the private zone was found to increase with the puffing rate whereas it was almost constant at the strike points (see Figure 11a). As for the power scan, the ions contribution to the inventory is rather low in the private zone (see Figure 11b). Moreover, the contribution of ions decreases rapidly at the strike points and represents only half of the surface concentration at 4×10^{21} molecule s^{-1}.

The inventory in the whole WEST divertor is computed from Equation (4). As for the power scan, the divertor

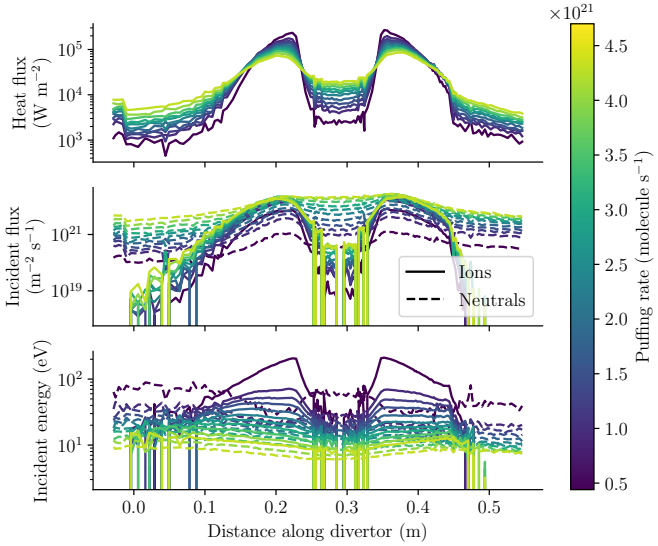

Figure 8: Distribution of heat flux, particle flux and particle energy along the WEST divertor computed by SOLEDGE3X-EIRENE with a puffing rate varying from $4.4 \times 10^{20}\,\mathrm{s}^{-1}$ to $4.7 \times 10^{21}\,\mathrm{s}^{-1}$ with 0.45 MW of input power.

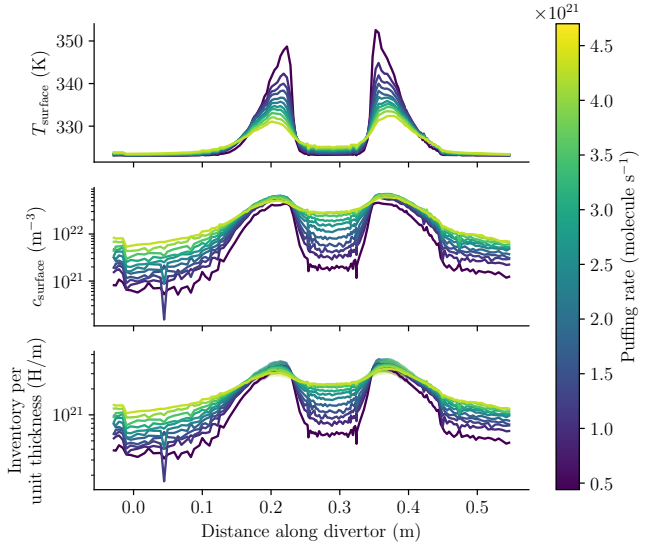

Figure 9: Distribution of surface temperature T_{surface}, surface concentration c_{surface} and inventory along the WEST divertor with a puffing rate varying from $4.4 \times 10^{20}\,\mathrm{s}^{-1}$ to $4.7 \times 10^{21}\,\mathrm{s}^{-1}$ with 0.45 MW of input power.

inventory increased as the power 0.2 of the puffing rate (see Figure 10). The maximum inventory was found to be 5×10^{23} H at 4.7×10^{21} molecule s^{-1}.

The divertor inventory was found to increase as a square root of time.

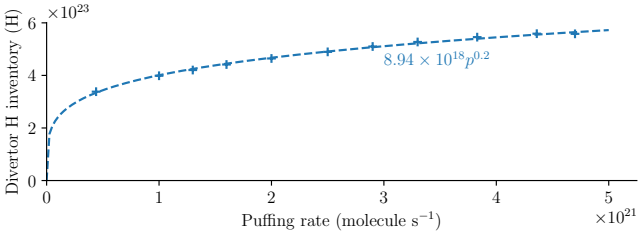

Figure 10: Evolution of the WEST divertor inventory as a function of puffing rate.

3.2. ITER

The heat flux was maximum at the outer strike point reaching 20 MW m^{-2} (see Figure 12). The neutral particles incident energy was found to be at least one order of magnitude lower than that of the ions.

Peak temperatures at strike points increased when decreasing the divertor neutral pressure (see Figure 13). The peak temperature at the outer strike point reached 2000 K at 2 Pa and more than 1000 K at the inner strike point which is in accordance with the results obtained by Pitts *et al* [19]. This is consistent with the higher heat flux observed at the outer strike point (see Figure 12). The inventory in the whole divertor is computed as follow:

$$\mathrm{inv}_{\mathrm{divertor}} = N_{\mathrm{cassettes}} \cdot \left(N_{\mathrm{PFU-IVT}} \cdot \int \mathrm{inv}_{\mathrm{IVT}}(x)\,dx + N_{\mathrm{PFU-OVT}} \cdot \int \mathrm{inv}_{\mathrm{OVT}}(x)\,dx\right) \quad (5)$$

with $N_{\mathrm{cassettes}} = 54$ the number of cassettes, $N_{\mathrm{PFU-IVT}} = 16$ and $N_{\mathrm{PFU-OVT}} = 22$ the number of plasma facing units per cassette in the inner and outer targets respectively, $\mathrm{inv}_{\mathrm{IVT}}$ and $\mathrm{inv}_{\mathrm{OVT}}$ the hydrogen inventory profile along the inner and outer targets respectively and x the distance along the targets.

The inventory in the outer target was found to be nearly twice that of the inner target. This is greatly explained by the larger number of plasma facing units in the outer target and therefore a greater exposed surface. The global inventory increases with the divertor neutral pressure and a slight roll-over is observed above 7 Pa (see Figure 14). This roll-over is consistent with the results obtained in [19]. It is mainly due to the surface temperature variations near the outer strike point inducing variation in the near strike point inventory (see Figure 13b).

The inventory increase was found to be more important in the outer vertical target. This was explained by the fact that the plasma is more detached at the inner target. Therefore the surface temperature reduction is more significant in the outer vertical target and the surface concentration is increased (see Figure 13b).

The maximum inventory was found at around 7 Pa and was approximately 14 g of H which is well below the ITER in-vessel safety limit of tritium (1 kg), especially considering only half of this quantity will be tritium. This is especially true considering that this was for a very long exposure time of 10^7 s which corresponds to 25 000 pulses of 400 s.

The inventory at the inner and outer strike points globally increases with the divertor neutral pressure (see Figure

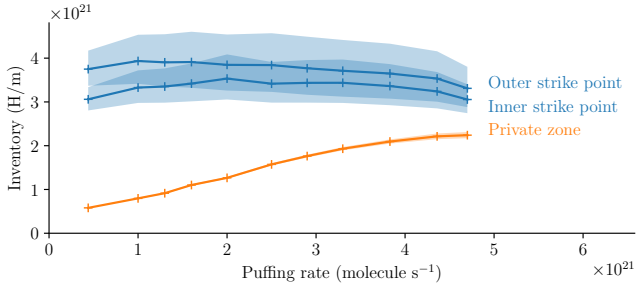

(a) Inventory per unit thickness after 10^7 s of exposure. The area corresponds to the 95% confidence interval.

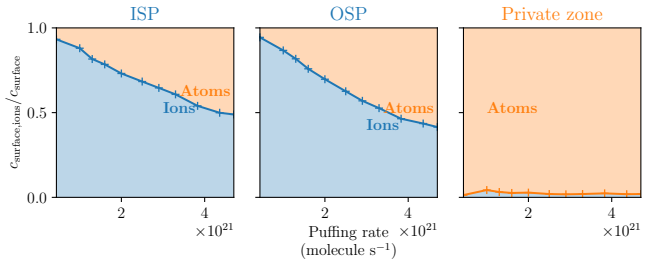

(b) Contribution of ions to the surface concentration of H. ISP and OSP stand for Inner Strike Point and Outer Strike Point respectively.

Figure 11: H retention in WEST at the strike points and in the private zone as a function of puffing rate with 0.45 MW of SOL input power.

15a). The contribution of ions to the surface concentration at the inner strike point is around 50 % and tends to decrease with increasing neutral pressure (see Figure 15b). At low divertor neutral pressure, the contribution of ions at the outer strike point is around 90 % and tends to decrease with increasing neutral pressure. This can be explained by the fact that in both inner and outer targets, the integrated flux of ions decreases with increasing neutral pressure whereas the integrated flux of atoms increases, leading to a greater proportion of neutral particles.

For all divertor neutral pressures, the temporal evolution of the divertor inventory is approximately the same (see Figure 16). The additional inventory per 400 s discharge was found to decrease with time. Past 300 discharges, the additional inventory per discharge decreases with the number of discharges. The maximum is around 5 mg/discharge between 30 and 100 discharges.

4. Conclusion

Fuel retention of both the WEST and the ITER divertors was studied. The technique developed in [4] has been applied to various divertor exposures. The influence of key control parameters such as the SOL input power, the puffing rate and the divertor neutral pressure was investigated. This technique can be applied to any reactor using the monoblock concept to shied the divertor/limiter. however, some reactors like JET do not use the monoblock design and this technique is therefore not applicable.

It was shown that the inventory in WEST increases as the power 0.3 of the SOL input power and as the power 0.2 of the puffing rate. The inventory in the ITER divertor was found to first increase with the neutral pressure up to 7 Pa then decrease, though the variation was smoother. The inventory in the outer vertical target of the ITER divertor is twice that of the inner vertical target. These results were in good agreement with the observations made in [19].

However, it should be noted that for these simulations both machines do not operate in the same regime. While WEST operates at low SOL input power, ITER operates at high input power with a high recycling divertor. These differences in the operation regime can explain different trends.

The underlying monoblock model has also a few limitations, as detailed in [4]. First, the set of trapping parameters that was used may not be relevant for every region of the divertor. These properties can however be estimated from experimental work [23, 24]. The accuracy of the results could therefore be improved by running a new batch of FESTIM monoblock simulations with different trapping parameters like neutron-induced traps. The impact of edge localised modes is assumed to be negligible for very long exposure times [25].

Then, this model does not take into account retention in Be co-deposited layers. These are expected to be the main driver for H retention in ITER [26]. Estimations of the retention rate in these layers range from 100 mg to 300 mg per 400 s shot [27]. The retention rate computed in this study is much lower and remains below 5 mg per discharge. However, this work is still relevant for full-W environments like WEST and DEMO.

Additionally, the FESTIM results used in this model are 2D simulations. It could be argued that 3D edge effects due to desorption from the gaps between the monoblocks would decrease the estimated inventory. The current assumption is therefore conservative and is a worst-case scenario. However, the influence of 3D edge effects on the monoblock inventory and outgassing fluxes will be investigated in future work.

Acknowledgements

The project leading to this publication has received funding from Excellence Initiative of Aix-Marseille University - A*Midex, a French "Investissements d'Avenir" programme as well as from the French National Research Agency (Grant No. ANR-18-CE05-0012). This work has been carried out within the framework of the EUROfusion Consortium and has received funding from the Euratom research and training programme 2014-2018 and 2019-2020 under grant agreement No 633053. The views and opinions expressed herein do not necessarily reflect those of the European Commission. The views and opinions expressed herein do not necessarily reflect those of the ITER Organization.

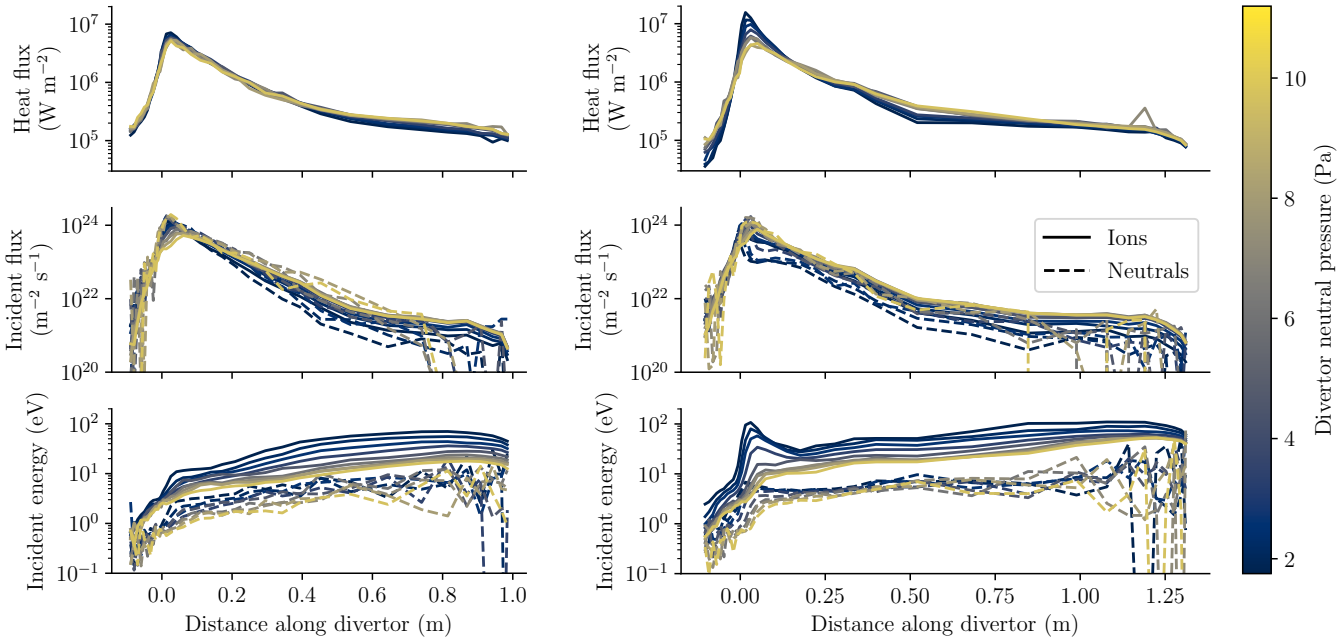

(a) Inner vertical target

(b) Outer vertical target

Figure 12: Heat flux, particle flux and particle energy along ITER divertor computed by SOLPS with neutral pressures varying from 2 Pa to 11 Pa.

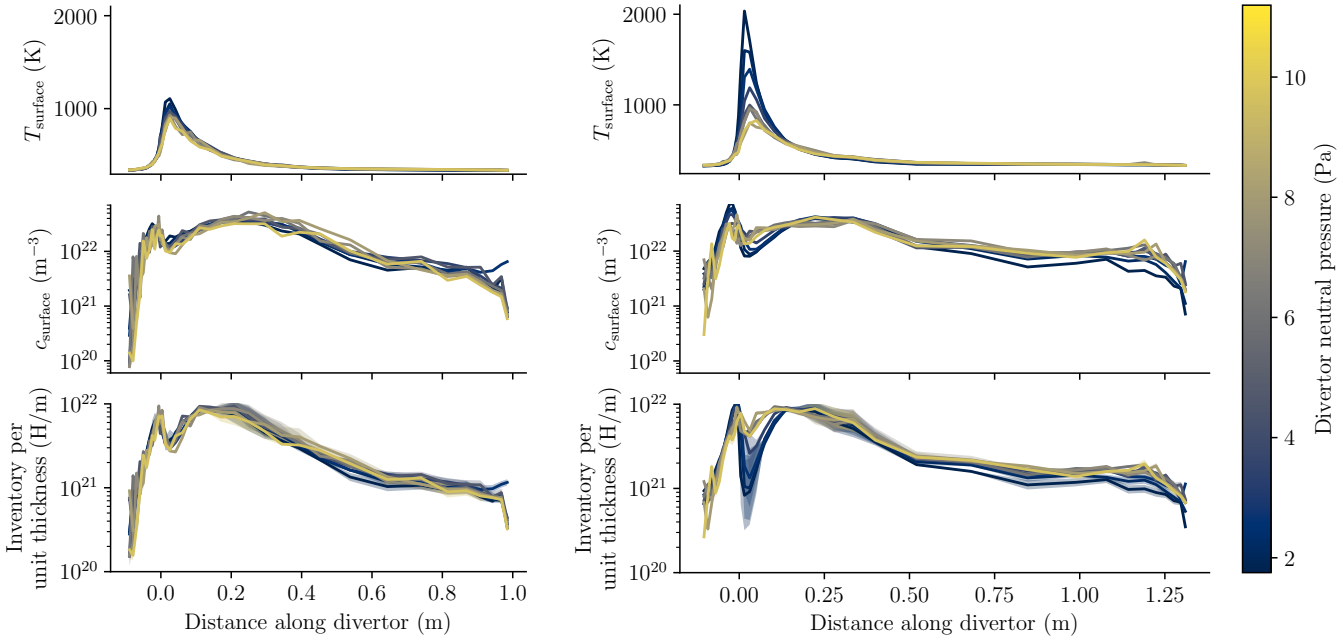

(a) Inner vertical target

(b) Outer vertical target

Figure 13: Surface temperature, surface concentration and inventory along ITER divertor with neutral pressures varying from 2 Pa to 11 Pa. Area corresponds to the 95% confidence interval.

References

[1] G. De Temmerman, T. Hirai, and R. A. Pitts. The influence of plasma-surface interaction on the performance of tungsten at the ITER divertor vertical targets. *Plasma Physics and Controlled Fusion*, 60(4):044018, March 2018. Publisher: IOP Publishing.

[2] C. Grisolia. Plasma wall interaction during long pulse operation in Tore Supra. *Journal of Nuclear Materials*, 266-269:146–152, March 1999.

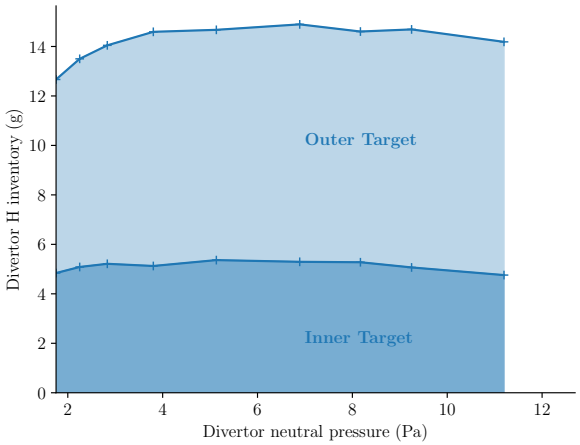

Figure 14: Hydrogen inventory in the ITER divertor as a function of neutral pressure after 10^7 s of exposure (approximately 25 000 discharges).

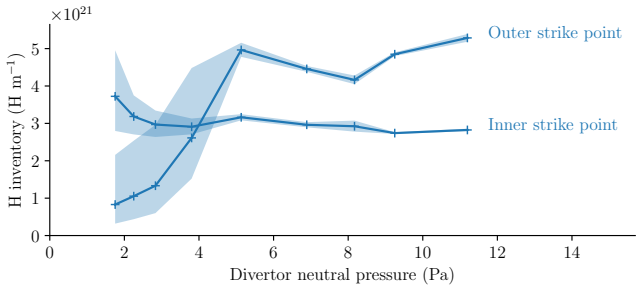

(a) Inventory per unit thickness after 10^7 s of exposure (approximately 25 000 discharges). Area corresponds to the 95% confidence interval.

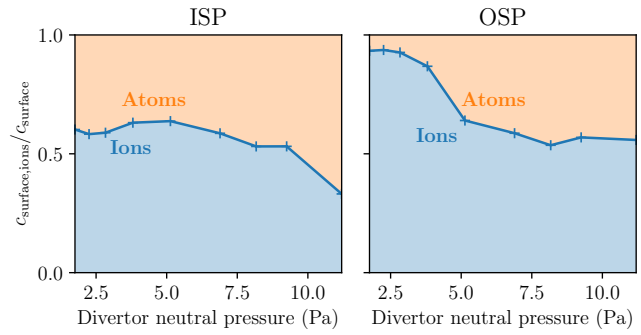

(b) Contribution of ions to the surface concentration of H.

Figure 15: H retention at the strike points (defined as maximum temperature) as a function of the divertor neutral pressure.

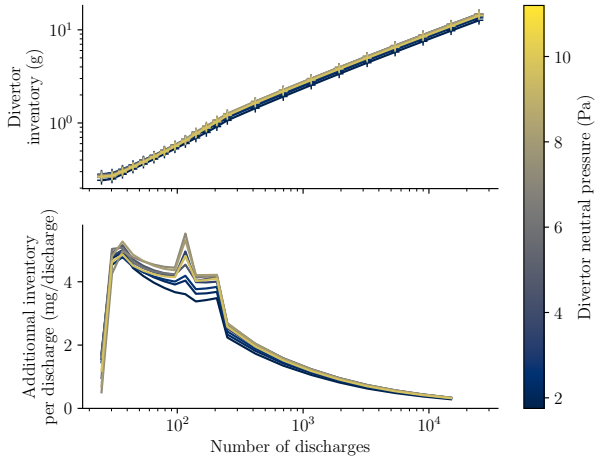

Figure 16: Evolution of the H inventory of the ITER divertor with the number of 400 s discharges.

[3] Sandeep Kumar Dwivedi and Manish Vishwakarma. Hydrogen embrittlement in different materials: A review. *International Journal of Hydrogen Energy*, 43(46):21603–21616, November 2018.

[4] Rémi Delaporte-Mathurin, Etienne Hodille, Jonathan Mougenot, Gregory De Temmerman, Yann Charles, and Christian Grisolia. Parametric study of hydrogenic inventory in the ITER divertor based on machine learning. *Scientific Reports*, 10(1):17798, October 2020. Number: 1 Publisher: Nature Publishing Group.

[5] Rémi Delaporte-Mathurin, Etienne Hodille, Jonathan Mougenot, Yann Charles, Gregory De Temmerman, Floriane Leblond, and Christian Grisolia. Influence of interface conditions on hydrogen transport studies. *Nuclear Fusion*, 61(3):036038, 2021.

[6] J. Denis, J. Bucalossi, G. Ciraolo, E. A. Hodille, B. Pégourié, H. Bufferand, C. Grisolia, T. Loarer, Y. Marandet, and E. Serre. Dynamic modelling of local fuel inventory and desorption in the whole tokamak vacuum vessel for auto-consistent plasma-wall interaction simulations. *Nuclear Materials and Energy*, 19:550–557, May 2019.

[7] James Dark, Rémi Delaporte-Mathurin, Yann Charles, Etienne A. Hodille, Christian Grisolia, and Jonathan Mougenot. Influence of hydrogen trapping on WCLL breeding blanket performances (submitted to Nuclear Fusion). 2021.

[8] E. A. Hodille, E. Bernard, S. Markelj, J. Mougenot, C. S. Becquart, R. Bisson, and C. Grisolia. Estimation of the tritium retention in ITER tungsten divertor target using macroscopic rate equations simulations. *Physica Scripta*, T170:014033, October 2017.

[9] Rémi Delaporte-Mathurin, Etienne A. Hodille, Jonathan Mougenot, Yann Charles, and Christian Grisolia. Finite element analysis of hydrogen retention in ITER plasma facing components using FESTIM. *Nuclear Materials and Energy*, 21:100709, December 2019.

[10] Sofiane Benannoune, Yann Charles, Jonathan Mougenot, Monique Gaspérini, and Greg De Temmerman. Multidimensional finite-element simulations of the diffusion and trapping of hydrogen in plasma-facing components including thermal expansion. *Physica Scripta*, T171:014011, January 2020.

[11] M. Richou, F. Gallay, B. Böswirth, I. Chu, M. Lenci, Th Loewenhoff, A. Quet, H. Greuner, G. Kermouche, E. Meillot, G. Pintsuk, E. Visca, and J. H. You. Realization of high heat flux tungsten monoblock type target with graded interlayer for application to DEMO divertor. *Physica Scripta*, T170:014022, October 2017. Publisher: IOP Publishing.

[12] Chris Bowman. C-bowman/inference-tools: 0.5.3 release, April 2020.

[13] H. Bufferand, P. Tamain, S. Baschetti, J. Bucalossi, G. Ciraolo, N. Fedorczak, Ph. Ghendrih, F. Nespoli, F. Schwander, E. Serre, and Y. Marandet. Three-dimensional modelling of edge multi-component plasma taking into account realistic wall geometry. *Nuclear Materials and Energy*, 18:82–86, January 2019.

[14] E. Kaveeva, V. Rozhansky, I. Senichenkov, E. Sytova, I. Veselova, S. Voskoboynikov, X. Bonnin, R. A. Pitts, A. S.

Kukushkin, S. Wiesen, and D. Coster. SOLPS-ITER modelling of ITER edge plasma with drifts and currents. *Nuclear Fusion*, 60(4):046019, March 2020. Publisher: IOP Publishing.

[15] Etienne A. Hodille, Rémi Delaporte-Mathurin, J. Denis, M. Pecovnik, E. Bernard, Y. Ferro, R. Sakamoto, Y. Charles, J. Mougenot, A. De Backer, C. S. Becquart, S. Markelj, and C. Grisolia. Modelling of hydrogen trapping, diffusion and permeation in divertor monoblocks under ITER-like conditions (submitted to Nuclear Fusion). 2021.

[16] G. Ciraolo, A. Thin, H. Bufferand, J. Bucalossi, N. Fedorczak, J. P. Gunn, J. Y. Pascal, P. Tamain, C. Gil, A. Gouin, O. Meyer, P. Devynck, S. Vartanian, C. C. Klepper, E. Serre, F. Nespoli, A. Gallo, Y. Marandet, and J. Rosato. First modeling of strongly radiating WEST plasmas with SOLEDGE-EIRENE. *Nuclear Materials and Energy*, 20:100685, August 2019.

[17] F. Imbeaux, S. D. Pinches, J. B. Lister, Y. Buravand, T. Casper, B. Duval, B. Guillerminet, M. Hosokawa, W. Houlberg, P. Huynh, S. H. Kim, G. Manduchi, M. Owsiak, B. Palak, M. Plociennik, G. Rouault, O. Sauter, and P. Strand. Design and first applications of the ITER integrated modelling & analysis suite. *Nuclear Fusion*, 55(12):123006, October 2015. Publisher: IOP Publishing.

[18] Jae-Sun Park, Xavier Bonnin, and Richard Pitts. Assessment of ITER divertor performance during early operation phases. *Nuclear Fusion*, 61(1):016021, December 2020. Publisher: IOP Publishing.

[19] R. A. Pitts, X. Bonnin, F. Escourbiac, H. Frerichs, J. P. Gunn, T. Hirai, A. S. Kukushkin, E. Kaveeva, M. A. Miller, D. Moulton, V. Rozhansky, I. Senichenkov, E. Sytova, O. Schmitz, P. C. Stangeby, G. De Temmerman, I. Veselova, and S. Wiesen. Physics basis for the first ITER tungsten divertor. *Nuclear Materials and Energy*, 20:100696, August 2019.

[20] James F. Ziegler, M. D. Ziegler, and J. P. Biersack. SRIM – The stopping and range of ions in matter (2010). *Nuclear Instruments and Methods in Physics Research Section B: Beam Interactions with Materials and Atoms*, 268(11):1818–1823, June 2010.

[21] Rémi Delaporte-Mathurin, James Dark, Hao Yang, and E. A. Hodille. IRFM/divHretention source code Github repository https://github.com/IRFM/divHretention, June 2021. original-date: 2021-02-02T15:25:50Z.

[22] Remi Delaporte-Mathurin. divHretention: Tool to estimate H retention in tokamak divertors, v0.1.3 PyPi distribution.

[23] Floriane Leblond, E. A. Hodille, S. Vartanian, M. Payet, R. Delaporte-Mathurin, J. Mougenot, Y. Charles, E. Bernard, and C. Grisolia. Permeation and trapping of hydrogen in Eurofer97 (accepted in Nuclear Materials and Energy) 10.1016/j.nme.2021.101062. 2021.

[24] Rémi Delaporte-Mathurin, Etienne A. Hodille, Jonathan Mougenot, Yann Charles, and Christian Grisolia. Parametric optimisation based on TDS experiments for rapid and efficient identification of hydrogen transport materials properties. *Nuclear Materials and Energy*, page 100984, March 2021.

[25] K. Schmid. Diffusion-trapping modelling of hydrogen recycling in tungsten under ELM-like heat loads. *Physica Scripta*, T167:014025, January 2016. Publisher: IOP Publishing.

[26] Gregory De Temmerman, Kalle Heinola, Dmitriy Borodin, Sebastijan Brezinsek, Russell P. Doerner, Marek Rubel, Elżbieta Fortuna-Zaleśna, Christian Linsmeier, Daisuke Nishijima, Kai Nordlund, Michael Probst, Juri Romazanov, Elnaz Safi, Thomas Schwarz-Selinger, Anna Widdowson, Bastiaan J. Braams, Hyun-Kyung Chung, and Christian Hill. Data on erosion and hydrogen fuel retention in Beryllium plasma-facing materials. *Nuclear Materials and Energy*, 27:100994, June 2021.

[27] A. Khan, G. De Temmerman, S. W. Lisgo, X. Bonnin, H. Anand, M. A. Miller, R. A. Pitts, K. Schmid, and A. S. Kukushkin. WallDYN simulations of material migration and fuel retention in ITER low power H plasmas and high power neon-seeded DT plasmas. *Nuclear Materials and Energy*, 20:100674, August 2019.